OXFORD
SOT | Society of Toxicology
academic.oup.com/toxsci

Toxicological Sciences, 2025, **205(2),** 401–416
https://doi.org/10.1093/toxsci/kfaf033
Advance Access Publication Date: April 12, 2025
Research article

Establishing a context of use for three-dimensional cardiac tissue derived from human-induced pluripotent stem cell-derived cardiomyocytes using inotropes

Yoshiko Okai[1], Emily Pfeiffer Kaushik[2], Tomoya Sameshima[1], Nicole Feric[3], Rishabh Singh[3], Isabella Pallotta[3], Danielle R. Bogdanowicz[3], Marietta M. Gustilo[3], Kosuke Harada[1], Kevin S. Baker[2], Tadahiro Shinozawa[1,*]

[1]Drug Safety Research and Evaluation, Takeda Pharmaceutical Company Limited, Kanagawa 251-8555, Japan
[2]Drug Safety Research and Evaluation, Takeda Development Center Americas, Inc, Cambridge, MA 02139, United States
[3]Valo Health, Inc, New York, NY 10016, United States

*Corresponding author: Drug Safety Research and Evaluation, Takeda Pharmaceutical Company Limited, 26-1, Muraoka-Higashi 2-chome, Fujisawa, Kanagawa 251-8555, Japan. E-mail: tadahiro.shinozawa@takeda.com

Abstract

Safety attrition due to drug-induced inotropic changes remains a significant risk factor for drug development. Mitigating these events during early screening remains challenging. Several in vitro predictive models have been developed to address these issues, with varying success in detecting drug-induced inotropic changes. In this study, we compared traditional two-dimensional human-induced pluripotent stem cell-derived cardiomyocytes (2D hiPSC-CMs) with three-dimensional engineered cardiac tissues (3D ECTs) to assess their ability to detect drug-induced inotropic changes in 17 drugs with known mechanisms of action. The models were exposed to various test compounds, and their responses were evaluated by measuring either the active force or maximum contraction speed. The 3D ECTs successfully detected all the tested positive inotropes, whereas the 2D hiPSC-CMs failed to detect the 2 compounds. Both models demonstrated high predictability for negative inotropy and showed similar results for detecting non-active compounds, except for higher concentrations of phentolamine, zimelidine, and tamsulosin. Irregular beating was less likely to occur in the 3D ECTs, suggesting that 3D ECTs provided superior detection of contractility compared to 2D hiPSC-CMs. Genetic analysis revealed a more mature phenotype for the 3D ECTs compared to the 2D hiPSC-CMs, and the compound-related target expression was comparable to that in the adult human heart tissues. The 3D ECTs captured inotropic changes more accurately and thus represented a more translatable model than the 2D hiPSC-CMs. Overall, contractility assessment using the 3D ECTs could be advantageous for profiling candidate compounds and mechanistic investigations of hemodynamic changes during in vivo or clinical studies.

Keywords: cardiac contractility; 3D engineered cardiac tissue; 2D hiPSC-CMs; drug-induced inotropic change

Introduction

Safety concerns are among the highest contributors to drug attrition during preclinical and clinical development. A review detailing the causes of attrition of 812 orally developed compounds between 2000 and 2010 showed that 308 compounds (51% of all 605 terminated compounds) were discontinued because of non-clinical toxicology and clinical safety concerns (Waring et al. 2015). Cardiotoxicity is a major driver of drug attrition and withdrawal throughout the development process owing to safety concerns (Laverty et al. 2011; Siramshetty et al. 2016). Among the top 200 prescribed drugs in the United States, 85 are labeled with adverse drug reactions or black-box warnings related to cardiovascular toxicity (Fuentes et al. 2018). Consequently, preclinical assessments to identify cardiac liabilities in the early phases of drug development are crucial to reduce cardiotoxicity-related attrition.

Cardiac muscle contraction is the most fundamental function of the heart, and unexpected drug-induced modification of cardiac muscle contraction (i.e. cardiac inotropic changes) is a risk factor for cardiovascular-related attrition. Both positive and negative inotropic effects can be harmful to patients with heart disease and healthy individuals (Wallis et al. 2015). For example, itraconazole is a synthetic antifungal agent that may be associated with congestive heart failure owing to its negative inotropic effects, as evidenced by animal and clinical pharmacology studies (Ahmad et al. 2001). Clinical trials of positive inotropes, such as milrinone and amrinone, have failed to improve the clinical outcomes of heart failure and have resulted in worse clinical outcomes (Ahmad et al. 2019). Positive inotropic agents, such as β-receptor agonists, α1-receptor agonists, and phosphodiesterase-3 inhibitors, increase intracellular [Ca^{2+}], oxygen consumption, and fuel depletion in energy-starved hearts, leading to subsequent myocardial damage (Rajapreyar et al. 2014). Therefore, understanding drug-induced inotropic potential is important for drug development and preemptive mitigation of adverse effects.

We previously developed a non-invasive, video-based assessment of drug-induced inotropic changes using motion-field imaging (Okai et al. 2020). This technology utilizes high-resolution and high-frame-rate video to perform continuous, real-time

measurements of the contractile behavior of two-dimensional (2D) cultured human-induced pluripotent stem cell-derived cardiomyocytes (hiPSC-CMs). Although the assay demonstrated high clinical predictability for drug-induced inotropic effects, it was unable to detect the expected effects of some compounds, possibly due to the limitations imposed by the immature phenotype of hiPSC-CMs, which may affect both the predictability and translatability of the results. To overcome this limitation, micro engineered heart tissues with more mature properties (e.g. non-spontaneous beating, T-tubule development, and increased contractile force) have been developed over the last several years (Ribeiro et al. 2019). The Biowire II platform consists of an array of polystyrene microwells with 2 parallel flexible polymer wires fixed at each end. This platform enables the growth of thin cylindrical tissues, akin to human trabeculae, suspended between 2 wires, facilitating the quantification of contractile forces (Zhao et al. 2019). Three-dimensional (3D) engineered cardiac tissues (ECTs) developed using hiPSC-CMs and cardiac fibroblasts, generated on the Biowire II platform, display a more mature phenotype than 2D hiPSC-CMs and identify inotropic changes induced by several drugs with different underlying mechanisms during contractility assessment (Feric et al. 2019; Qu et al. 2020). However, the ability of drugs to modulate contractility has not been fully investigated using this platform, and this model has not been directly compared with a 2D model to evaluate the translatability of drug responses.

In the present study, we tested 17 compounds with known mechanisms of action, including negative inotropes, positive inotropes, and non-active compounds, to evaluate their effects on the contractility of the 3D ECTs generated using the Biowire II platform. Additionally, we compared the responses of the 3D ECTs to these test compounds with those of 2D hiPSC-CMs. Finally, we investigated the global gene expression in the 3D ECTs and 2D hiPSC-CMs to understand the mechanistic differences in drug responses between the 2 models and to determine the feasibility of using these models for practical drug screening applications.

Materials and methods

Test compounds

The following drugs were used to measure contractility in the 3D ECTs: captopril, cimetidine, sildenafil, and tamsulosin, purchased from Cayman Chemical Company (Ann Arbor, MI, United States), and pravastatin, zimelidine, acetylsalicylic acid (aspirin), amrinone, glyburide (glibenclamide), haloperidol, itraconazole, mexiletine hydrochloride (mexiletine), phentolamine hydrochloride (phentolamine), phenylephrine hydrochloride (phenylephrine), pimobendan, and (±)-propranolol hydrochloride (propranolol), purchased from Sigma-Aldrich (St Louis, MO, United States). Dimethyl sulfoxide (DMSO) and isoproterenol were also purchased from Sigma-Aldrich and used as the vehicle and positive control, respectively.

The following compounds were purchased for contractility measurement studies using the 2D hiPSC-CMs: glibenclamide and haloperidol from Fujifilm Wako Pure Chemicals (Osaka, Japan); pimobendan, amrinone, mexiletine, itraconazole, captopril, cimetidine, pravastatin, phentolamine, zimelidine, tamsulosin, and sildenafil from Sigma-Aldrich; and aspirin, DL-phenylephrine hydrochloride, isoproterenol hydrochloride, and propranolol from Tokyo Chemical Industry Company Limited (Tokyo, Japan).

All test drugs were dissolved in DMSO (Fujifilm). The final DMSO concentrations for contractility measurements using the 2D hiPSC-CMs were 0.1% v/v (low concentration), 0.2% v/v (mid concentration), 0.3% v/v (high concentration), and 0.4% v/v (highest concentration). The final DMSO concentrations for contractility measurements using the 3D ECTs were 0.001% v/v (low concentration), 0.01% v/v (medium concentration), and 0.1% v/v (high concentration) for the three-concentration measurements, and 0.003% v/v (low concentration), 0.01% v/v (mid concentration), 0.03% v/v (high concentration), and 0.1% v/v (highest concentration) for the four-concentration measurements. The concentrations, mechanisms of action, and target-related genes of the tested drugs are listed in Table 1.

Generation of 3D ECTs

The 3D ECTs were generated using iCell® Cardiomyocytes^2 (FUJIFILM Cellular Dynamics International, Madison, WI, United States) and human ventricular cardiac fibroblasts (Lonza, Allendale, NJ, United States) on the Biowire II platform, as described previously (Feric et al. 2019; Zhao et al. 2019). Briefly, a collagen/Matrigel/fibrin hydrogel was prepared by mixing 75% v/v collagen hydrogel (rat tail collagen, 3 mg/mL, Corning, AZ, United States; 1× M199; Matrigel, 15% v/v, Corning; deionized H_2O; NaOH, 0.01 N; $NaHCO_3$, 0.22 mg/mL) and 25% fibrinogen hydrogel (fibrinogen, 33 mg/mL, Sigma-Aldrich; HEPES, 20 mM; NaCl, 0.9% w/v). Then, 1×10^5 viable iCell Cardiomyocytes^2 and 1×10^4 human ventricular cardiac fibroblasts were suspended in the hydrogel. The suspended cells were seeded on the Biowire II platform, containing polystyrene microwells with parallel poly (octamethylene maleate (anhydride) citrate) (POMaC) wires. The ECTs were subjected to an electrical field stimulation protocol using biphasic pulses for a duration of 2 ms at twice the excitation threshold for 10 weeks. The ECTs were assessed for automaticity (spontaneous beat rate), force–frequency relationship (active force at 1 to 4 Hz), and post-rest potentiation. Post-rest potentiation was assessed by measuring the first beat at 1 Hz, followed by rapid pacing and a 10-s rest. ECTs with minimal spontaneous activity that exhibited a positive force–frequency relationship and post-rest potentiation were assessed for their responsiveness to 100 nM isoproterenol. Tissue batches that showed a robust (at least 3-fold vs. baseline) β-adrenergic response to 100 nM isoproterenol were used for test compound assessments. The use of 3D ECTs was approved by the ethics committee of Takeda Pharmaceutical Company Limited.

Treatment of 3D ECTs and contractility acquisition

The contractility of the 3D ECTs was measured using a previously described non-invasive optical technique (Feric et al. 2019; Zhao et al. 2019; Qu et al. 2020). The contractility of the suspended ECTs was measured by tracking the deflection of the fluorescent POMaC wires as a function of time. The 3D ECTs were transferred to an environmental chamber (5% CO_2, 37°C) under field electrical stimulation at 1 Hz (2 ms pulse duration, monophasic, at 200% of the excitation threshold voltage). After equilibration of the 3D ECTs in the environmental chamber for 30 min, the first baseline video was captured for 30 s. Subsequently, one-third of the tissue culture medium volume was pipetted twice from the chamber containing the tissues to equilibrate them with the shear stress induced by the procedure. A second 30-s baseline video was captured 10 min after the addition of the culture medium to analyze the effects of the test compounds. Each test compound was dissolved in DMSO and applied to the medium in

Table 1. Summary profile for reference compounds tested in motion field imaging assay.

Non-active compounds		
Compound	**Mechanism of action**	
Aspirin	Cyclooxygenase inhibitor	
Captopril	Angiotensin-converting enzyme inhibitor	
Cimetidine	H2-receptor antagonist	
Pravastatin	HMG-CoA reductase inhibitor	
Phentolamine	Nonselective α adrenoceptor antagonist	
Zimelidine	Selective serotonin reuptake inhibitor	
Sildenafil	PDE-5 inhibitor	
Tamsulosin	α-1 adrenoceptor antagonist	
Negative inotropes		
Compound	**Mechanism of action**	**Potential target genes related to inotropic changes**
Itraconazole	Inhibition of lanosterol 14α-demethylase	*SCN5A* (Qu et al. 2013)
Propranolol	Nonselective β receptor antagonist	*ADRB1*, *ADRB2*
Mexiletine	Na^+ channel blocker	*SCN5A*
Haloperidol	Dopamine D2-receptor antagonist	*CACNA1C*, *SIGMAR1* (Novakova et al. 1995; Hatip-Al-Khatib and Bolukbasi-Hatip 2002)
Positive inotropes		
Compound	**Mechanism of action**	**Potential target genes related to inotropic changes**
Isoproterenol	Nonselective β adrenergic receptor agonist	*ADRB1*, *ADRB2*
Phenylephrine	α-1 and ß-1 adrenergic receptor agonist	*ADRA1A*, *ADRA1D*, *ADRA1B*, *ADRB1*
Glibenclamide	K_{ATP} channel inhibitor	*ABCC8*, *KCNJ11*, *KCNJ8*, *ABCC9*
Amrinone	PDE-3 inhibitor	*PDE3A*. *PDE3B*
Pimobendan	Calcium sensitizer with PDE-3 inhibition	*TNNC1*, *TNNT2*, *TNNI3*, *RYR1*, *PLN*, *ATP2A2*, *PDE3A*, *PDE3B*

the tissue wells to achieve the desired final concentration. One-third of the medium volume was then pipetted twice for gentle mixing. The tissue was incubated with the test drugs or DMSO vehicle control for 15 min, after which a 30-s video was captured. This procedure was repeated for all subsequent concentrations (from lowest to highest), such that each tissue was incubated with 3 or 4 increasing concentrations of the test compounds. For each treatment, the number of tissues tested (n) ranged from 6 to 9, and each tissue was exposed to a single compound. Data analysis was performed by analyzing the videos using custom software that tracks the displacement of the POMaC wires to measure ECT contractility. The maximum contraction force represents the active force generated. The active force at each dose was normalized by dividing the active force in the presence of the compound by the baseline active force in the same tissue.

Statistical analysis for determining effects on 3D ECT-generated force

Data are presented as the mean ± SD. The F-test was used to compare the test article group and the time-matched vehicle control group to test for homogeneity of variance. Student's t-test and Aspin–Welch's test were used when the variances between the 2 groups were homogeneous and heterogeneous, respectively. Statistical significance was set at $P < 0.05$. These calculations were performed using EXSUS ver.8.0 (SAS 9.3, EPS Corporation, Tokyo, Japan).

Preparation of 2D cultured hiPSC-CMs for contractility assessment

Cryopreserved cardiomyocytes derived from human iPS cells (iCell® Cardiomyocytes; Cellular Dynamics International, Fujifilm, Tokyo, Japan) were purchased and prepared following the manufacturer's instructions. To obtain a sheet of cardiomyocytes with spontaneous and synchronous activity, the cells were re-plated on a small area (approximately 2 μm in diameter) of 12-well plates as previously described (Okai et al. 2020). Briefly, the cells were thawed using iCell® Cardiomyocytes Plating Medium (Cellular Dynamics International) and then plated in 2 wells of a gelatin-coated six-well plate (BD, Franklin Lakes, NJ, United States) at a density of 2 to 3×10^6 cells/well. Approximately 48 h after the initial plating, the plating medium was replaced with iCell® Cardiomyocytes Maintenance Medium (Cellular Dynamics International). On day 7 after plating, hiPSC-CMs were re-plated on a small area (approximately 3 mm in diameter) coated with 20 μL of fibronectin (5 μg/mL; Corning, New York, NY, United States) in 12-well plates (Eppendorf, Hamburg, Germany) at a density of 4.0×10^4 cells in 20 μL. The cells were incubated at 37°C with 5% CO_2 for 3.5 to 6 h prior to adding 1.5 mL of the maintenance medium to each well. The cells were cultured at 37°C under 5% CO_2 in 12-well plates for 5 to 9 days until recording was performed. Half of the medium volume (750 μL) was changed every 2 to 3 days throughout the study. The evening before recording, the maintenance medium in each well was replaced with 2 mL of fresh serum-containing medium used throughout the recording. Before recording, the 12-well plates were equilibrated in a mini-incubator (37°C, 5% CO_2) attached to the motion-field imaging system stage for >30 min before the commencement of data acquisition. The use of hiPSC-CMs was approved by the ethics committee of Takeda Pharmaceutical Company Limited.

Contractility acquisition using 2D cultured hiPSC-CMs

High-resolution block-matching-based optical flow was used to assess contractility in 2D cultured hiPSC-CMs, as previously

described (Hayakawa et al. 2012). Briefly, video images of beating hiPSC-CMs were captured as sequential phase-contrast images with a 4× objective at 150 frames/s frame rate and a resolution of 2048 × 2048 pixels (2.8 mm × 2.8 mm) using the SI8000 cell motion-field imaging system (Sony Corporation, Tokyo, Japan). The moving images were captured thrice for 5 s at 4-min intervals to confirm steady beating. Fifteen minutes after the addition of 2 μL of maintenance medium, a baseline video of each well was captured continuously for 10 s. Subsequently, stock solutions of the test compounds, prepared in DMSO at a 1,000-fold target concentration, were cumulatively applied from the lowest to the highest concentration to achieve the target concentrations. The cells were incubated with each concentration of each compound for 15 min, and a video was captured continuously for 10 s. Data from 4 to 5 wells were obtained for each test compound.

The contractile behavior of hiPSC-CMs recorded in the video was analyzed using a block-matching algorithm, and bimodal waveforms consisting of contractions and relaxations were obtained by plotting the average motion vectors against time, as previously described (Hayakawa et al. 2012). The maximum contraction speed, defined as the peak amplitude of the contraction waveform, was obtained using Sony SI8000 analysis software and used as an index of contractility.

To evaluate the effects of the test compounds, wells in which the beats per minute coefficient of variation (CoV) of the 3 pre-assay recordings did not exceed 5% were used. The absolute maximum contraction speed values at each concentration were normalized and represented as the percentage change from the baseline values, which were obtained after sham treatment (treatment with culture medium). If irregular beating and/or quiescence were observed at certain concentrations of the test drug, the maximum contraction speed values were not analyzed at those concentrations. The upper and lower cutoff values of fold change in maximum contraction speed were set at 1.08-fold and 0.92-fold, respectively, based on the variation range and mean ± 3SD of the background data for the vehicle control (DMSO, $n = 20$), respectively (data not shown). The minimum effective concentration (MEC) and concentrations for a 1.08-fold increase or 0.92-fold decrease in maximum contraction speed were calculated using a four-parameter log equation with Model 204 in the XLFit software (IDBS Limited, Woking, United Kingdom).

Global gene expression analysis

Total RNA was extracted from untreated 3D ECTs that qualified similarly for contractility assessment using an RNAdvance Tissue Kit (A32645; Beckman Coulter, Brea, CA, United States), according to the manufacturer's protocol. DNase digestion was performed using the DNase reagent included in the RNeasy Micro Kit (74004; QIAGEN, Gaithersburg, MD, United States). Total RNA was also extracted from untreated 2D hiPSC-CMs on day 14 of culture, under the same conditions applied during motion-field imaging video recording, using either the QIAGEN RNeasy Micro Kit (74004; QIAGEN, Gaithersburg, MD, United States) or the QIAGEN RNeasy Mini Kit (74004; QIAGEN, Gaithersburg, MD, United States), following the manufacturers' protocols. DNase digestion was performed using the DNase reagent included in the extraction kit. Three total RNA samples from adult human tissues were purchased from Thermo Fisher Scientific (Waltham, MA, United States), BioChain (Newark, CA, United States), and Takara Bio Inc. (Mountain View, CA, United States). All 3 samples were obtained from normal heart tissues. The BioChain sample is from the ventricle. The extracted and purified RNA samples were subjected to Ion AmpliSeq Human Transcriptome Analysis (Ion Torrent, Thermo Fisher, United States) by Axcelead Drug Discovery Partners, Inc. (Fujisawa, Japan). The RNA-seq count data for the samples were pre-processed using the Voom transformation method (Law et al. 2014).

Heart contraction-related genes were selected according to the Gene Ontology (GO) annotation (https://amigo.geneontology.org/amigo/landing). Of the 227 genes included in the GO database under the term "heart contraction" (GO: 0060047), 222 showed expression levels greater than zero in at least one of our study samples. The expression patterns of these 222 genes were analyzed to investigate the molecular similarities between the 3D ECTs, 2D hiPSC-CMs, and human heart tissues in terms of heart contractility.

Omics Studio (QIAGEN, Venlo, Netherlands) was used to perform the principal component analysis (PCA) of the RNA sequencing data (18,650 genes) and the hierarchical clustering analysis of the selected heart contraction-related genes and samples. A correlation algorithm was applied to calculate the gene distance, and hierarchical trees were created based on the complete linkage method. In the hierarchical clustering view, each row represents a sample, and each column represents a gene. A visual color code was used, with magenta and cyan indicating relatively high and low expression levels, respectively.

Results

Characterization of 2D hiPSC-CMs and 3D ECTs for contractility baseline values and response to isoproterenol

The baseline contractility measurements were determined before testing the responses of the 3D ECTs and the 2D hiPSC-CMs to experimental compounds. Figure 1A represents force (converted from displacement) versus time in the 3D ECTs, whereas Fig. 1B represents the derivative of displacement (velocity) versus time in the 2D hiPSC-CMs. The active force, which represents the contraction peak amplitude, was used as an index of contractility in the 3D ECTs, whereas the maximum contraction speed was used as an index of contractility in the 2D hiPSC-CMs. The pre-treatment baseline values of the active force in the 3D ECTs were 4.8 ± 3.9 μN (mean ± SD, $N = 134$, from 0.32 to 26 μN) and CoV for the baseline was 81% (Fig. 1C). The culture medium treatment baseline values of maximum contraction speed in the 2D cultured hiPSC-CMs were 11 ± 1.2 μm/s (mean ± SD, $N = 89$, from 8.8 to 14 μm/s), and CoV for the baseline was 11% (Fig. 1D). Next, we characterized the 2D hiPSC-CMs and the 3D ECTs for their canonical response to the well-known β-adrenergic receptor agonist isoproterenol, considered a gold standard and previously tested in both models (Feric et al. 2019; Okai et al. 2020). The physiological response to this positive inotropy was determined using the active force and maximum contraction speed. The positive inotropic effect of isoproterenol was detected in the 3D ECTs and the 2D hiPSC-CMs at below 0.1 and 0.35 nM, respectively, as the MEC. Interestingly, the fold changes from baseline values in the 3D ECTs were larger than those in the 2D hiPSC-CMs (Fig. 1E and F). Overall, the 3D ECTs exhibited a reasonable physiological baseline and responded to a positive inotrope similarly to the 2D hiPSC-CMs.

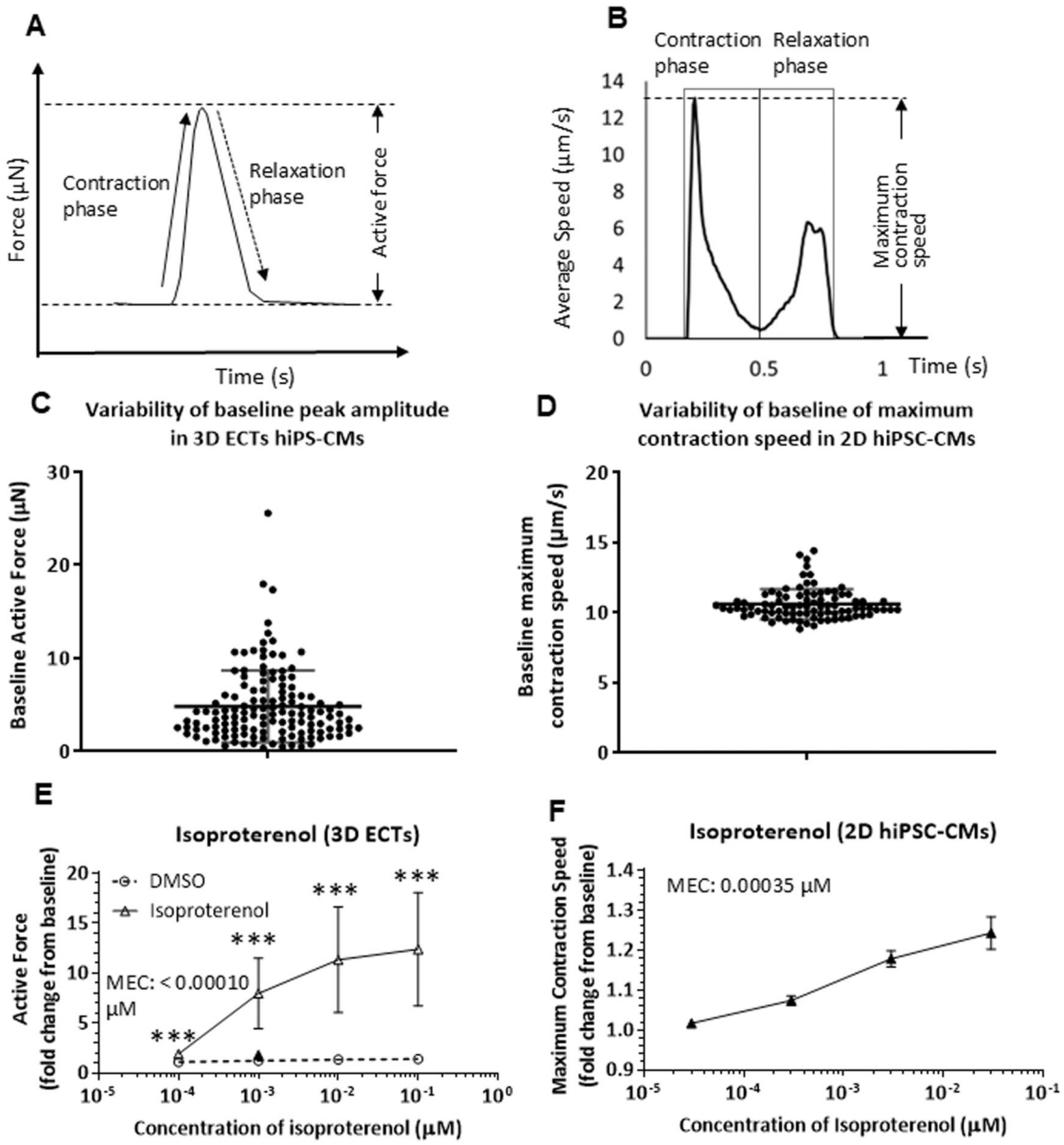

Fig. 1. Characteristics of contractility in the 3D ECTs and 2D hiPSC-CMs. A) Representative waveform plotting force (converted from displacement) vs. time in the 3D ECTs. B) Typical motion waveforms plotting speed (the derivative of displacement) vs. time in the 2D hiPSC-CMs. C) Variability in baseline active force pre-treatment. D) Variability in baseline maximum contraction speed values after treatment with maintenance medium. E) Effects of isoproterenol on the active force in the 3D ECTs. F) Effects of isoproterenol on the maximum contraction speed in the 2D hiPSC-CMs. MEC, minimum effective concentration. ***, significantly different from vehicle control (***$P < 0.001$).

Effects of various drugs on active force in 3D ECTs and maximum contraction speed of 2D hiPSC-CMs

To evaluate the contractility of the 3D ECTs and the 2D hiPSC-CMs, we tested 17 compounds, including 4 positive inotropes (pimobendan, amrinone, glibenclamide, and phenylephrine), 4 negative inotropes (propranolol, mexiletine, itraconazole, and haloperidol), and 8 non-active compounds (aspirin, captopril, cimetidine, pravastatin, phentolamine, zimelidine, tamsulosin, and sildenafil), which were selected from the drugs used for the validation of the motion-field imaging assay system in our previous 2D hiPSC-CM study (Okai et al. 2020). The data for the 29 compounds, including isoproterenol, are summarized in Table 2.

Among the positive inotropes, phenylephrine (α-1 adrenoceptor agonist) increased the active force and maximum contraction speed in a concentration-dependent manner in the 3D ECTs and the 2D hiPSC-CMs, respectively, as shown in representative contractile traces (Fig. 2A and B). The MEC of phenylephrine in the 3D ECTs and the 2D hiPSC-CMs were 0.30 and 0.056 μM, respectively (Fig. 2C and D). The 3D ECTs showed an increase in active force after treatment with pimobendan (a calcium sensitizer with pyridine phosphodiesterase 3 [PDE3] inhibition activity), and the MEC was 3.0 μM (Fig. 2E). However, pimobendan did not affect the maximum contraction speed of the 2D hiPSC-CMs (Fig. 2F). Amrinone (a PDE3 inhibitor) showed a trend toward an increase in active force at 30 μM in the 3D ECTs, though this change was not statistically significant (Fig. 2G). In contrast, no effect was observed in the 2D hiPSC-CMs at concentrations up to 100 μM (Fig. 2H). In both the 3D and the 2D models, no effect was observed after treatment with glibenclamide (a K_{ATP} channel

Table 2. Summary of results of 16 tested compounds.

		3D ECTs			2D hiPSC-CMs		
Compound	**Effects in human**	**Test concentrations (μM)**	**Effects on active force**	**MEC (μM)**	**Test concentrations (μM)**	**Effects on MCS**	**MEC (μM)**
Positive inotropes							
Isoproterenol	Positive inotrope	0.00010, 0.0010, 0.010, 0.10	Increase	<0.00010	0.000030, 0.00030, 0.0030, 0.030	Increase	0.00035
Phenylephrine	Positive inotrope	0.030, 0.30, 3.0	Increase	0.30	0.030, 0.10, 0.30, 1.0	Increase	0.056
Pimobendan	Positive inotrope	0.30, 3.0, 30	Increase	3.0	3.0, 10, 30, 60	No effect	>60
Amrinone	Positive inotrope	1.0, 10, 30	Trend increase	30	3.0, 10, 30, 100	No effect	>100
Glibenclamide	Positive inotrope	1.0, 10, 100	No effect	>100	3.0, 10, 30, 100	No effect	>100
Negative inotropes							
Propranolol	Negative inotrope	0.30, 3.0, 30	Decrease	3.0	0.30, 1.0, 3.0, 10	Decrease	3.8
Mexiletine	Negative inotrope	0.10, 1.0, 10	Decrease	1.0	1.0, 3.0, 10, 30	Decrease	13
Itraconazole	Negative inotrope	0.030, 0.30, 3.0	Decrease	3.0	0.30, 1.0, 3.0[a], 10[a]	Decrease	0.31
Haloperidol	Negative inotrope (in dog)	0.030, 0.30, 3.0	Increase (0.30 μM)/ decrease (3.0 μM)	0.30	0.010, 0.030, 0.10, 0.30[b]	No effect	>0.10
Non-active compounds							
Aspirin	No effect	3.0, 30, 300	No effect	>300	10, 30, 100, 300	No effect	>300
Captopril	No effect	3.0, 10, 30, 100	No effect	>100	3.0, 10, 30, 100	No effect	>100
Cimetidine	No effect	3.0, 10, 30, 100	No effect	>100	3.0, 10, 30, 100	No effect	>100
Pravastatin	No effect	3.0, 10, 30, 100	No effect	>100	3.0, 10, 30, 100	No effect	>100
Phentolamine	No effect	0.30, 3.0, 30	Decrease	30	0.030, 0.10, 0.30, 1.0[b]	No effect	>0.30
Zimelidine	No effect	1.0, 3.0, 10, 30	Decrease	10	0.030, 0.10, 0.30[b], 1.0[b]	No effect	>0.10
Tamsulosin	No effect	0.30, 1.0, 3.0, 10	Decrease	3.0	0.30, 1.0, 3.0, 10[b]	No effect	>3.0
Sildenafil	No effect	3.0, 10, 30, 100	Increase	100	3.0, 10, 30, 100	Increase	34

[a] Quiescence was induced.
[b] Irregular beating was induced.
3D ECTs, three-dimensional engineered cardiac tissues; 2D hiPSC-CMs, two-dimensional cultured human-induced pluripotent stem cell-derived cardiomyocytes; MEC, minimum effective concentration.

inhibitor) (Fig. 2I and J). Overall, the positive inotropic effects of pimobendan and amrinone were detected in the 3D ECTs, but not in the 2D hiPSC-CMs, suggesting that the 3D ECTs perform better at detecting positive inotropy than the 2D hiPSC-CMs.

Among the negative inotropes evaluated in the 3D ECTs, propranolol (nonselective β receptor inhibitor) decreased the active force and maximum contraction speed in a concentration-dependent manner in the 3D ECTs and 2D hiPSC-CMs, respectively, as shown in representative contractile traces (Fig. 3A and B). The MEC of propranolol in the 3D ECTs and the 2D hiPSC-CMs was 3.0 and 3.8 μM, respectively (Fig. 3C and D). Additionally, the active force in the 3D ECTs and the maximum contraction speed in the 2D hiPSC-CMs decreased after treatment with mexiletine and itraconazole (Fig. 3E through H). The MECs of mexiletine in the 3D ECTs and the 2D hiPSC-CMs were 1.0 and 13 μM, respectively, whereas those of itraconazole were 3.0 and 0.31 μM, respectively. Haloperidol showed a bimodal effect in the 3D ECTs. Specifically, we observed an increase in active force at 0.30 μM, followed by a decrease at 3.0 μM (Fig. 3I). On the contrary, in the 2D hiPSC-CMs, haloperidol tended to decrease the maximum contraction speed at 0.1 μM without exceeding the threshold; however, the effect on the maximum contraction speed could not be evaluated at concentrations above 0.10 μM because of irregular beating induced by haloperidol (Fig. 3J). Overall, the negative inotropic effects of propranolol, mexiletine, and itraconazole were detected with comparable MECs in both the 3D ECTs and the 2D hiPSC-CMs, suggesting that both models could predict negative inotropy.

Among the non-active compounds, aspirin (a cyclooxygenase inhibitor) did not elicit any change in the active force in the 3D ECTs or the maximum contraction speed in the 2D hiPSC-CMs at concentrations up to 300 μM (Fig. 4A through D). No effects were observed on the active force in the 3D ECTs and the maximum contraction speed in the 2D hiPSC-CMs after treatment with captopril (ACE inhibitor; Fig. 4E and F), cimetidine (H_2-receptor antagonist; Fig. 4G and H), and pravastatin (HMG-CoA reductase inhibitor; Fig. 4I and J) at concentrations up to 100 μM. Phentolamine (nonselective α-adrenoceptor antagonist; Fig. 4K and L), zimelidine (selective serotonin reuptake inhibitor; Fig. 4M and N), and tamsulosin (selective α1 adrenoceptor antagonist; Fig. 4O and P) did not affect the active force in the 3D ECTs up to concentrations of 3.0, 3.0, and 1.0 μM, respectively, and did not affect the maximum contraction speed in the 2D hiPSC-CMs up to concentrations of 0.30, 0.10, and 3.0 μM, respectively. Notably, at higher concentrations, these compounds decreased the active force in the 3D ECTs. However, at high concentrations, we did not observe any decrease in the maximum contraction speed in the 2D hiPSC-CMs; instead, we observed irregular beating. Sildenafil increased the active force in the 3D ECTs and the maximum contraction speed in the 2D hiPSC-CMs; the MECs of sildenafil in the 3D ECTs and the 2D hiPSC-CMs were 100 and 34 μM, respectively (Fig. 4Q and R). Overall, the responses to non-active compounds, with the exception of higher concentrations of phentolamine, zimelidine, and tamsulosin, were similar in both models. However, the irregular beating was less likely to occur in the 3D ECTs, suggesting that the 3D ECTs perform better at evaluating contractility at higher concentrations than the 2D hiPSC-CMs.

An extensive literature review (Table S1) was conducted to identify free and total human effective plasma concentrations

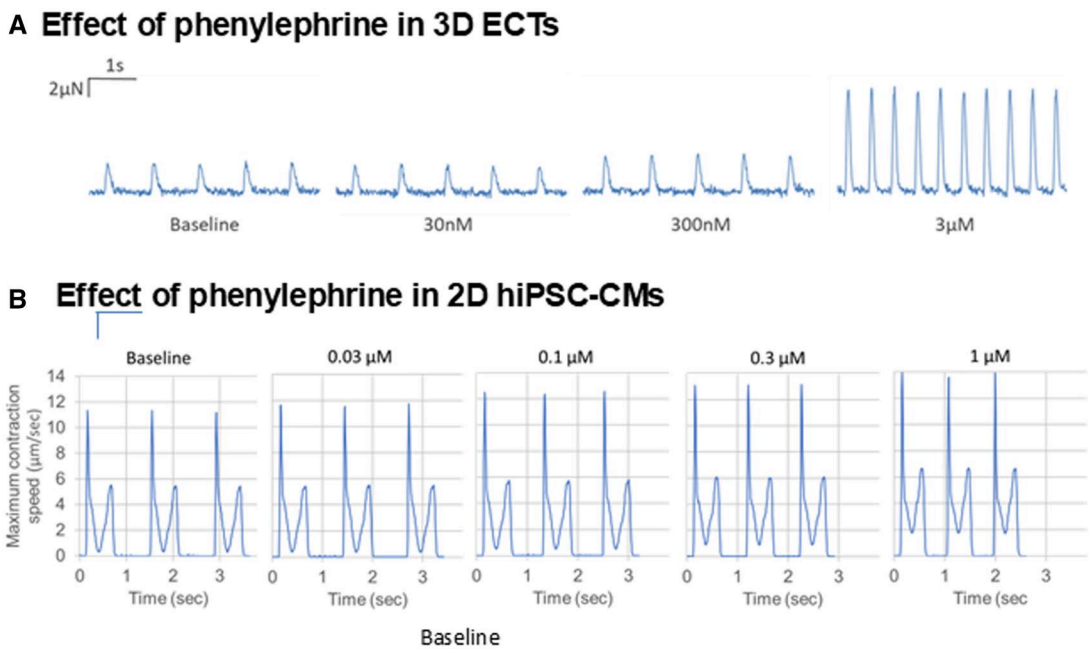

Fig. 2. Effect of positive inotropes on active force in 3D ECTs and maximum contraction speed in the 2D hiPSC-CMs. Percentage change from baseline in active force and maximum contraction speed 15 min after drug application. A) and B) Representative waveforms of phenylephrine-induced changes in the 3D ECTs and 2D hiPSC-CMs, respectively. C) and D) Effect of phenylephrine in the 3D ECTs and 2D hiPSC-CMs, respectively. E) and F) Effect of pimobendan on the 3D ECTs and 2D hiPSC-CMs, respectively. G) and H) Effect of amrinone on the 3D ECTs and 2D hiPSC-CMs, respectively. I) and J) Effect of glibenclamide on the 3D ECTs and 2D hiPSC-CMs, respectively. *, **, significantly different from vehicle control (*$P < 0.05$, **$P < 0.01$).

(ETPCs), allowing for comparison of MECs between the 3D ECTs (under serum-free conditions) and 2D hiPSC-CMs (under serum-containing conditions). The MEC-to-ETPC margins were calculated using free ETPC for the 3D ECTs and total ETPCs for the 2D hiPSC-CMs. Although this normalization approach provided some insights, it did not fully explain the MEC differences between the 2 models, which may be attributed to variations in drug responsiveness, cellular exposure, and protein-binding dynamics.

Analysis of gene expression associated with test compounds

To understand the mechanistic differences underlying the response to drugs between the 3D ECTs and the 2D hiPSC-CMs, we investigated global gene expression in both models. PCA of the RNA sequencing data (18,650 genes) was performed to visualize the relative similarities among the adult human heart tissues, 3D ECTs, and 2D hiPSC-CMs. PCA showed separation among all samples and clustering within the sample groups (Fig. S1A). Hierarchical clustering of the study samples based on the expression of heart contraction-related genes (GO: 0060047) showed that the 3D ECTs and 2D hiPSC-CMs clustered together, whereas the adult human heart tissue clustered separately (Fig. S1B). Following this initial quality control step, maturation-related genes were analyzed.

Maturation gene markers related to electrophysiology, calcium handling, contractility, and structure were identified using previously published reports (Machiraju and Greenway 2019; Karbassi et al. 2020) to compare gene expression related to maturation among the adult human heart tissues, 3D ECTs, and 2D hiPSC-CMs (Fig. 5A). Among the upregulated genes in mature cardiomyocytes, the expression levels of *RYR2*, *CAV3*, *CASQ2*, *ITPR3*, *S100A1*, *MYOM3*, and *KCNJ2* were higher in the 3D ECTs than in the 2D hiPSC-CMs. Additionally, the gene expression observed in the 3D ECTs was closer to that of the adult human heart tissue than that observed in the 2D hiPSC-CMs. In particular, the expression levels of *RYR2*, *CAV3*, *CASQ2*, *MYOM3*, and *KCNJ2* in the 3D ECTs were equivalent to or higher than those in the adult human heart tissue. Among the genes that were downregulated during the maturation process, lower expression levels were noted for *HCN4* in the 3D ECTs than in the 2D hiPSC-CMs. Among the fetal-to-adult isoform switching genes related to contractile proteins (e.g. *TNNI1* to *TNNI3*, *MYL7* to *MYL2*, and *MYL2* to *MYL4*), the 3D ECTs showed similar expression to that observed in the 2D hiPSC-CMs, but differed from that of the adult human heart tissue, with the exception of *MYH6* to *MYH7* switching. Notably, the expression of genes related to the isoform switch from *MYH6* to *MYH7* in the 2D hiPSC-CMs was more similar to that in the adult human heart tissue than to that in the 3D ECTs. The preference for the *MYH6* isoform by the 3D ECTs may be attributed to the fact that *MYH6* encodes the fast-twitch fiber and *MYH7* encodes the slow-twitch fiber, and that the 3D ECTs were conditioned at a physiologically high frequency, which selected *MYH6* over *MYH7* to obtain and maintain the maturation phenotype (Feric et al. 2019; Zhao et al. 2019). Taken together, the maturation gene analysis suggests that the 3D ECTs exhibit a mature phenotype similar to that of the adult human heart tissue.

Furthermore, genes related to inotropic changes among the 3 groups were considered. Fig. 5B shows the expression of potential genes related to the inotropic changes induced by the test compounds. Among the α-1 and β-adrenoreceptors targeted by propranolol, phenylephrine, and isoproterenol, higher expression levels were observed for *ADRA1A* and *ADRB1* in the 3D ECTs than in the 2D hiPSC-CMs, which showed expression levels closer to those in the adult human heart tissue. *PDE3A* and *PDE3B* are subfamily genes of the PDE3 family that are related to amrinone and

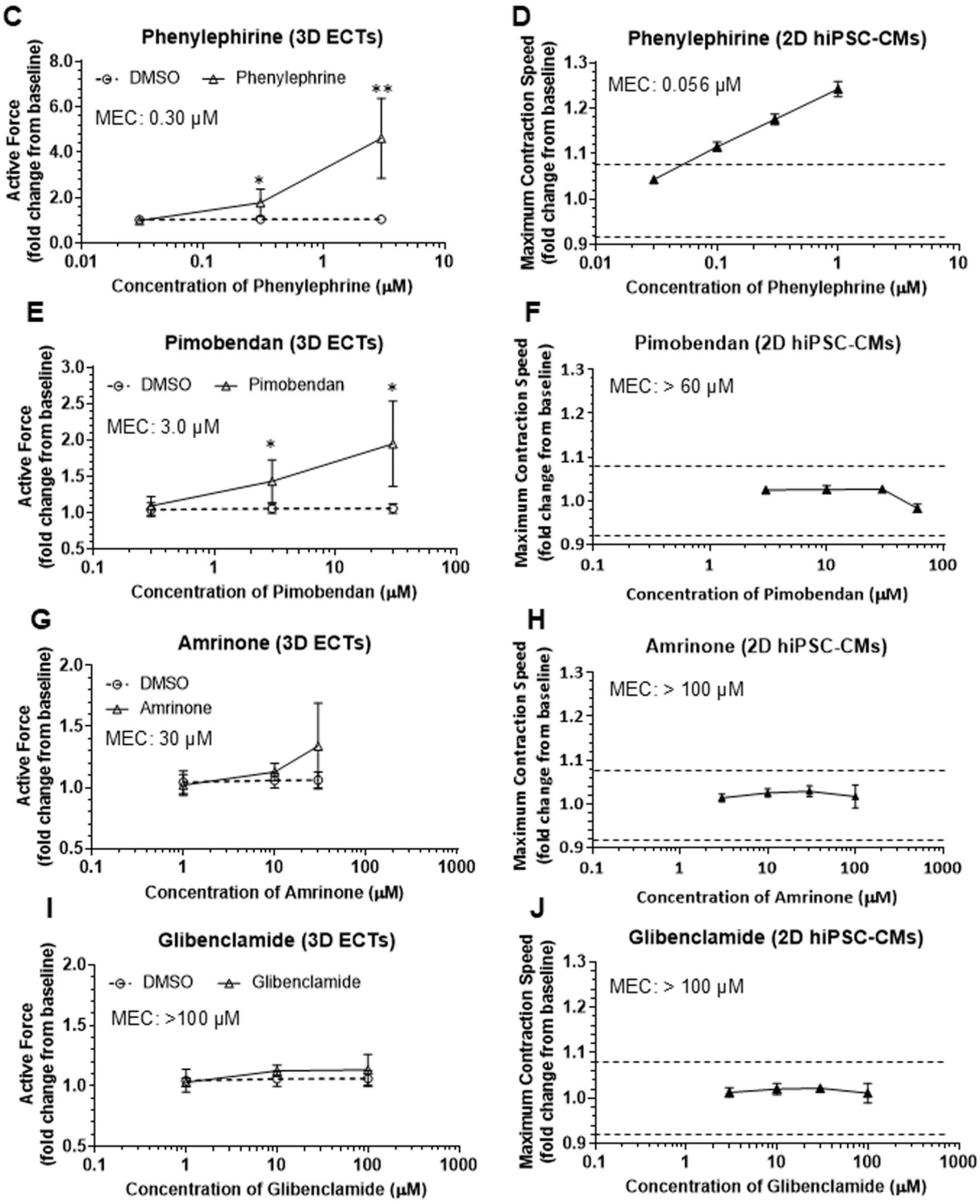

Fig. 2. Continued

pimobendan. The expression levels of *PDE3A* in the 3D ECTs and 2D hiPSC-CMs were approximately 1/4 and 1/200 of those observed in the adult human heart tissue, respectively. *PDE3B* expression in the 3D ECTs was lower than that in the 2D hiPSC-CMs and adult human heart tissues. *TNNC1* and *TNNT2* may be related to Ca2+ sensitizers (i.e. pimobendan), and their expression levels were similar in the 3D ECTs, the 2D hiPSC-CMs, and the adult human heart tissues. *ABCC8*, *KCNJ11*, *KCNJ8*, and *ABCC9* encode ATP-sensitive potassium (K_{ATP}) channels that are targeted by glibenclamide. *KCNJ8* expression was higher in the adult human heart tissue than in either the 3D ECTs or the 2D hiPSC-CMs. *SIGMAR1* encodes the sigma receptor, and *SIGMAR1* expression may be one of the causes of the inotropic changes induced by haloperidol. However, its expression level did not

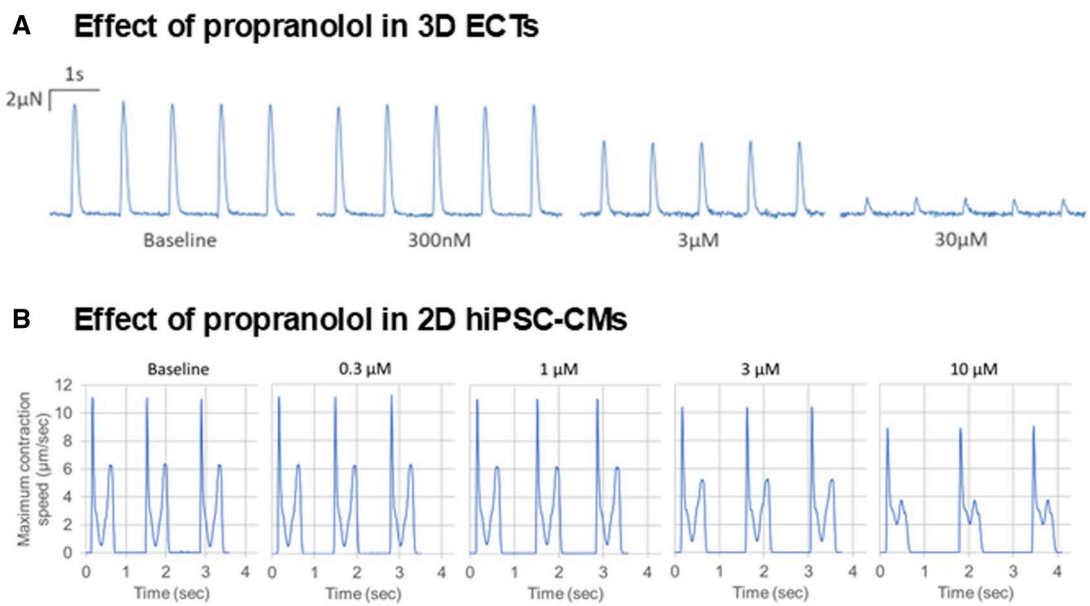

Fig. 3. Effect of negative inotropes on active force in 3D ECTs and maximum contraction speed in the 2D hiPSC-CMs. Percentage change from baseline in active force and maximum contraction speed 15 min after drug application. A) and B) Representative waveforms of propranolol-induced changes in the 3D ECTs and 2D hiPSC-CMs, respectively. C) and D) Effect of propranolol in the 3D ECTs and 2D hiPSC-CMs, respectively. E) and F) Effect of mexiletine in the 3D ECTs and 2D hiPSC-CMs, respectively. G) and H) Effect of itraconazole on the 3D ECTs and 2D hiPSC-CMs, respectively. I) and J) Effect of haloperidol on the 3D ECTs and 2D hiPSC-CMs, respectively. **, ***, significantly different from vehicle control (**$P < 0.01$, ***$P < 0.001$).

differ among the 3D ECTs, 2D hiPSC-CMs, and adult human heart tissue. The higher levels of *ADRB1*, *ADRA1A*, and *PDE3A* expressed in the 3D ECTs may enable better detection of both positive and negative inotropes. Overall, the expression levels of several genes related to maturation gene markers and potential targets of inotropic changes induced by the tested compounds in the 3D ECTs were closer to those in adult human heart tissue than in the 2D hiPSC-CMs.

Discussion

In our previous study, we developed an optimized 2D hiPSC-CMs screening system for assessing drug-induced inotropic effects (Okai et al. 2020). Although predictive and clinically translatable for certain drugs, its immature phenotype limited responsiveness, as evidenced by comparative gene expression analysis. To evaluate whether immaturity affects preclinical inotropic detection, we examined 3D ECTs generated from hiPSC-CMs mixed with cardiac fibroblasts in the Biowire II platform, display adult-like properties that are critical to understanding the translatability of experimental findings (Zhao et al. 2019) and respond to various inotropic compounds (Feric et al. 2019; Qu et al. 2020). This study compared the 3D ECTs and 2D hiPSC-CMs to contextualize 3D ECTs use in drug screening, with global gene expression analysis performed to explore differences in inotropic responses between models.

We observed key physiological differences between the 3D ECTs and the 2D hiPSC-CMs with the 3D ECTs exhibiting more adult-like properties, as evidenced by maturation-related gene expression compared to adult human heart tissue. *KCNJ2* and *HCN4*, which encode I_{K1} and I_f channels linked to automaticity, showed expression levels in the 3D ECTs were closer to the adult human heart tissues than the 2D hiPSC-CMs. This aligns with the minimal spontaneous activity in the 3D ECTs, because increased *KCNJ2* may lower resting potential, and decreased *HCN4* may reduce automaticity (Ma et al. 2011). *CAV3* (caveolin-3) expression was higher than in the 3D ECTs, matching the adult human heart tissue. This may explain levels, potentially contributing to t-tubule formation (Zhao et al. 2019). Since caveolin-3 aids t-tubule development, its reduced in the 2D hiPSC-CMs may explain their disrupted t-tubule structure (Parton et al. 1997; Bryant et al. 2018). Additionally, the 3D ECTs showed increased higher expression of calcium-handling genes (*RYR2*, *CASQ2*, *ITPR3*, *S100A1*) and structural genes (*MYOM3*), suggesting more mature contractile behavior (Ronaldson-Bouchard et al. 2018; Ernst et al. 2022). Overall, the 3D ECTs displayed a more mature phenotype than the 2D hiPSC-CMs, supporting their superior physiological relevance.

After genetic characterization, we tested the effects of inotropes and compared the responses between the 3D ECTs and 2D hiPSC-CMs. All tested positive inotropic drugs, except for glibenclamide, showed a response in the 3D ECTs. Positive inotropic changes of isoproterenol and phenylephrine were detected in both models, even though the 2D hiPSC-CMs had lower β-adrenergic receptor 1 (*ADBR1*) expression. In our previous study (Okai et al. 2020), we detected a positive inotropic effect of dobutamine (a selective β-adrenergic receptor 1 agonist), suggesting that effects mediated by a β-1 adrenergic receptor may be detected under low *ADBR1* expression. In contrast, the positive inotropic effects of amrinone and pimobendan, which are cardiotonic agents with the potential for PDE3 inhibition (van Meer et al. 2019), were detected in the 3D ECTs but not in the 2D hiPSC-CMs. This difference may be attributed to the expression of *PDE3A* rather than that of *PDE3B*. *PDE3A* inhibition reportedly alters basal cardiac contractility, whereas genetic ablation of *PDE3B* has no major effect on contractility (Beca et al. 2013; Movsesian et al. 2018). Pimobendan also mediates its positive inotropic effect by Ca^{2+}-sensitization, i.e. directly

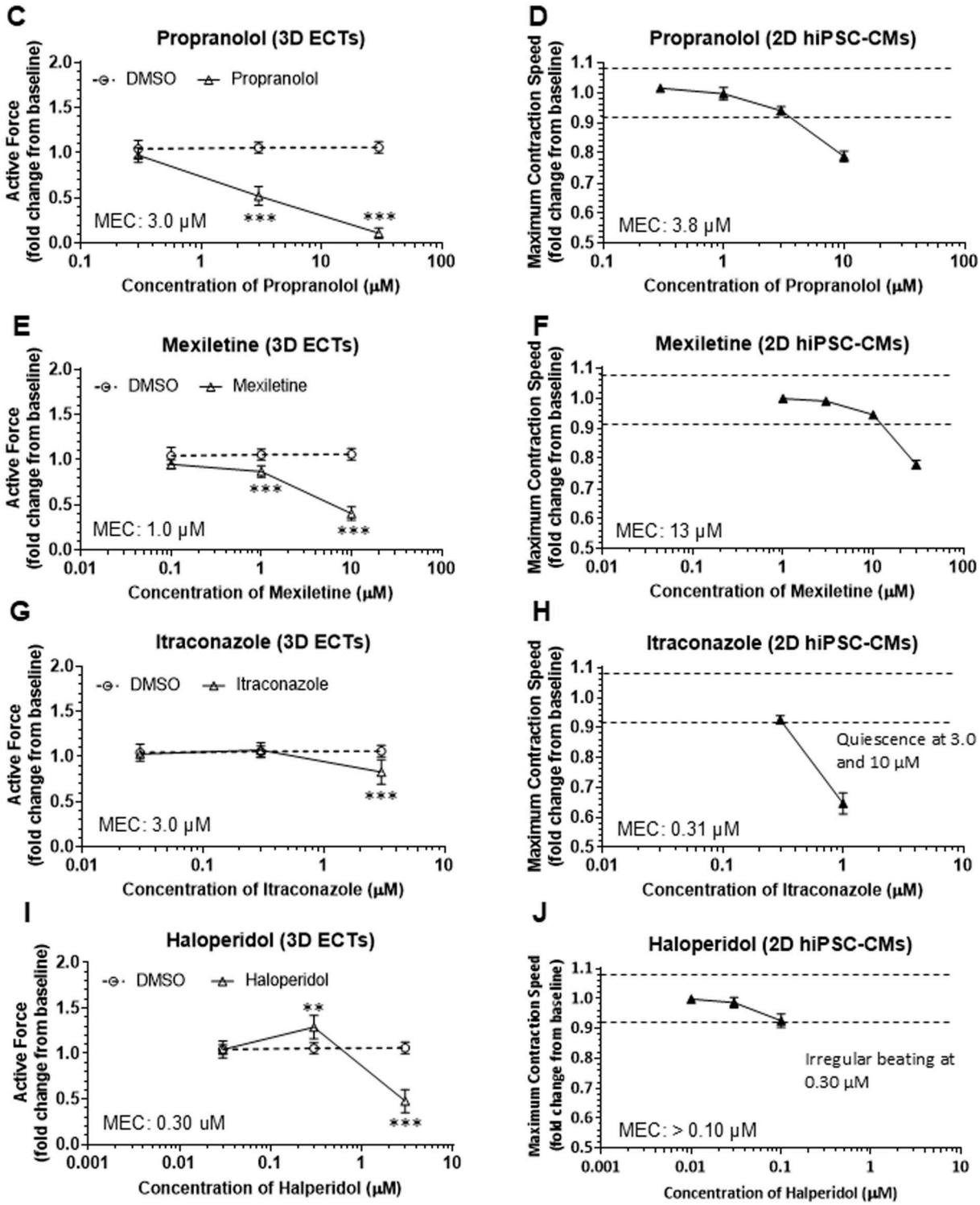

Fig. 3. Continued

increasing the affinity of the cardiac troponin C regulatory site for Ca^{2+} (Hori et al. 2019). Therefore, *RYR2* may also contribute to pimobendan responsiveness. *RYR2* and *PDE3A* expression levels in the 3D ECTs were closer to those in the adult human heart tissue than those in the 2D hiPSC-CMs. The inotropic effect of glibenclamide, a K_{ATP} channel inhibitor, was not observed in either model. Since the K_{ATP} channel opens only when cardiomyocytes are exposed to severe metabolic stress, such as anoxia, glibenclamide may not affect the channel in the closed state in hiPSC-CMs. Similarly, others reported that glibenclamide did not elicit any effect on the contractile behavior of hiPSC-CMs (Scott et al. 2014; Saleem et al. 2020; Tadano et al. 2021). Overall, the 3D ECTs, but not the 2D hiPSC-CMs, demonstrated sensitivity to PDE3 inhibition and Ca^{2+} sensitization, which might be explained by the differences in the expression of *PDE3A* and *RYR2*.

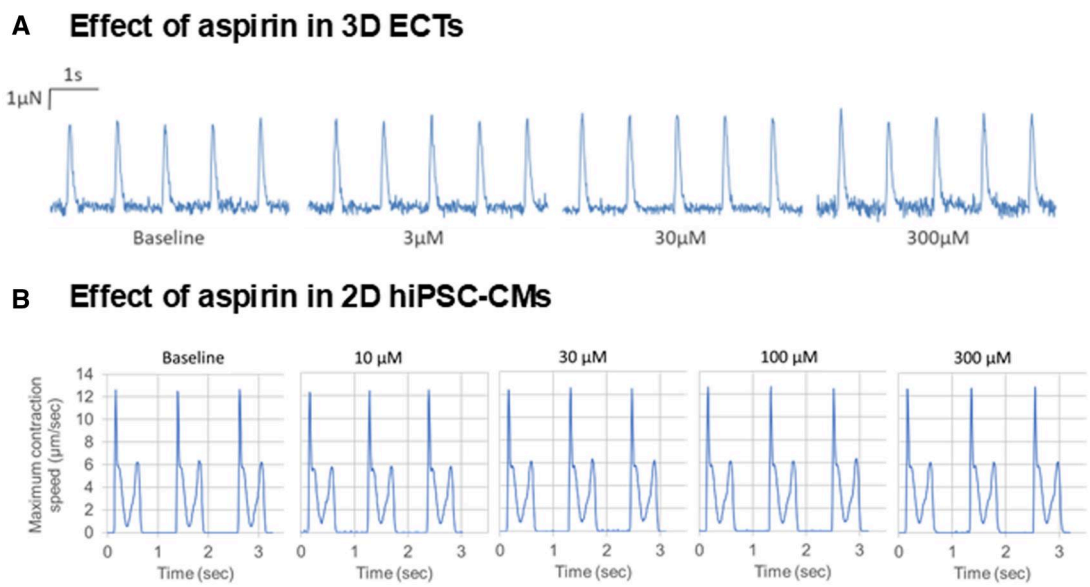

Fig. 4. Effect of negative inotropes on active force in 3D ECTs and maximum contraction speed in the 2D hiPSC-CMs. Percentage change from baseline in active force and maximum contraction speed 15 min after drug application. A) and B) Representative waveforms of aspirin-induced changes in the 3D ECTs and 2D hiPSC-CMs, respectively. C) and D) Effect of aspirin in the 3D ECTs and 2D hiPSC-CMs, respectively. E) and F) Effect of captopril on the 3D ECTs and 2D hiPSC-CMs, respectively. G) and H) Effect of cimetidine on the 3D ECTs and 2D hiPSC-CMs, respectively. I) and J) Effect of pravastatin on the 3D ECTs and 2D hiPSC-CMs, respectively. K) and L) Effect of phentolamine on the 3D ECTs and 2D hiPSC-CMs, respectively. M) and N) Effect of zimelidine on the 3D ECTs and 2D hiPSC-CMs, respectively. O) and P) Effect of tamsulosin on the 3D ECTs and 2D hiPSC-CMs, respectively. Q) and R) Effect of sildenafil on the 3D ECTs and 2D hiPSC-CMs, respectively. **, ***, significantly different from vehicle control (**$P < 0.01$, ***$P < 0.001$).

All negative inotropic drugs, except haloperidol, showed negative inotropic effects in both models. Although haloperidol was evaluated under conditions without dopamine tone, previous studies have shown that haloperidol reduces cardiac contractility by decreasing Ca^{2+} influx in isolated rabbit hearts (Hatip-Al-Khatib and Bolukbaşi-Hatip 2002). In our study, haloperidol induced a negative inotropic effect at 3 μM in the 3D ECTs, a concentration close to its $Ca_V1.2$ IC_{50} (1.3 μM, Ando et al. 2017), suggesting that $Ca_V1.2$ inhibition may underlie this effect. However, due to irregular beating, the highest testable concentration in the 2D hiPSC-CMs was 0.3 μM, at which no effect was observed. Given previous findings that paced samples exhibit reduced irregular beating compared to spontaneously beating samples (Hinata et al. 2022), electrically pacing may allow haloperidol's effects to be evaluated at higher concentrations. Additionally, a positive inotropic effect was observed at 0.3 μM in the 3D ECTs, though the underlying mechanism remains unclear. Regarding propranolol, the MECs in both models (~3 μM) were close to its $Na_V1.5$ IC_{50} (3 μM, Wang et al. 2010), suggesting that the negative inotropic effect observed in vitro might be driven by $Na_V1.5$ channel inhibition rather than β-adrenergic antagonism because our models lack sympathetic nerve fibers and endogenous norepinephrine.

Among the non-active compounds tested, aspirin, captopril, cimetidine, and pravastatin showed no effect on contractile behavior in either model. Sildenafil exhibited positive inotropic effects in both models, with MECs in the 3D ECTs reaching 2,273 times the free ETPC and in the 2D hiPSC-CMs reaching 31 times the total ETPC (Table S1). Sildenafil exerts a direct positive inotropic effect at concentrations approximately 20 to 200 times higher than the therapeutic level in isolated canine hearts (Lubna et al. 2016), suggesting that its observed effects in our models may also arise at supraphysiological exposures rather than being clinically relevant. Other compounds, such as zimelidine, tamsulosin, and phentolamine, exhibited negative inotropic effects in the 3D ECTs with MECs ranging from 408 to 20,270 times the free ETPC (Table S1), implying that these findings may reflect non-specific off-target effects rather than physiologically relevant responses. In contrast, in the 2D hiPSC-CMs, although tamsulosin did not affect contractility even at concentrations 81 times the total ETPC, phentolamine and zimelidine were only tested at concentrations similar to or below the total ETPC due to the induction of irregular beating (Table S1). Irregular beating in the 2D hiPSC-CMs is likely caused by hERG inhibition, which can confound contractility assessments. Phentolamine has a reported hERG IC_{50} of 0.85 μM, and zimelidine has been associated with an increased risk of Torsades de Pointes (Nachimuthu et al. 2012; Sube and Ertel 2017). Consequently, although the 2D hiPSC-CMs may yield fewer false-positive contractility changes, they may also miss true inotropic effects due to arrhythmic disruptions.

The most important consideration of this study was the application of contractility assessment using both models for drug discovery. Gene expression data and responses to the test compounds demonstrated that the 3D ECTs partially overcame the limitations of the immature phenotype of the 2D hiPSC-CMs. However, the 2D hiPSC-CMs exhibited less variability in baseline and drug-induced changes than those observed in the 3D ECTs, implying that a larger sample size may be necessary for performing contractility assays using the 3D ECTs. Recent studies have shown that aligning 2D hiPSC-CMs improves tissue maturation, enhances contractile gene expression, and refines responses to inotropic agents (Takada et al. 2022; Satsuka et al. 2024). These findings suggest that aligned 2D hiPSC-CMs may offer a more physiologically relevant alternative to traditional 2D monolayer cultures. However, although PDE3A expression was increased in

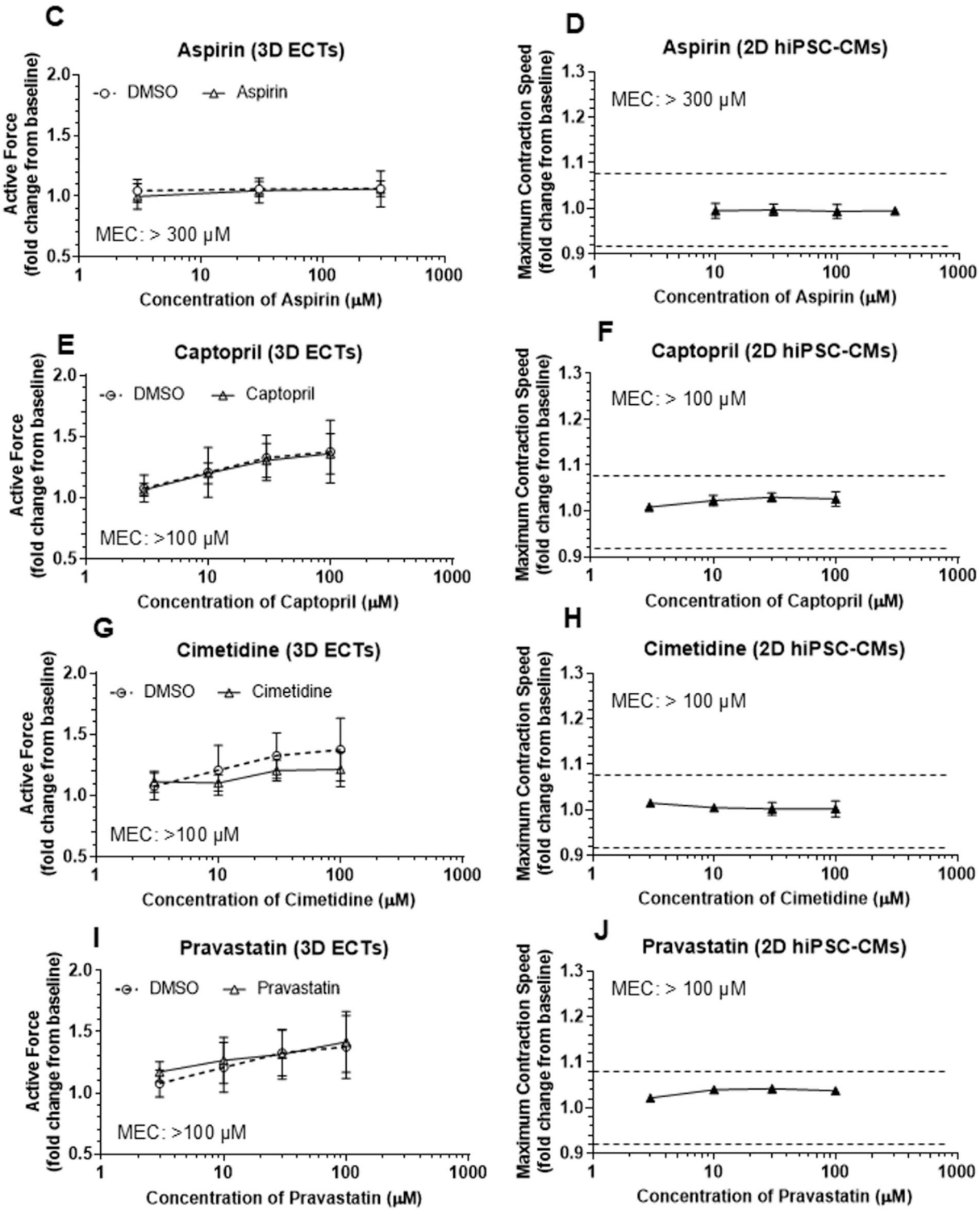

Fig. 4. Continued

the aligned hiPSC-CMs, milrinone's effect remained undetectable (Satsuka et al. 2024). In contrast, in studies using the same 3D ECT model, milrinone's positive inotropic effect was detectable (EC_{50} = 1.6 nM (Feric et al. 2019), suggesting that 3D ECTs may provide a more physiologically relevant assessment of contractility changes. Additionally, although the immature 2D hiPSC-CM model showed limitations, such as comprising a mixture of cardiomyocyte subtypes and a lack of other cardiac cell types (e.g. fibroblasts and endothelial cells), these characteristics could also be considered advantageous. Immature cells are easily dissociated, and homogeneous cardiomyocytes are more suitable for high-throughput assays and high-content imaging than mixed-cell populations (Burridge et al. 2016). Therefore, contractility assessment using 2D hiPSC-CMs might be suitable for drug screening in the earlier stages of drug development, whereas contractility assessment using 3D ECTs would be beneficial for

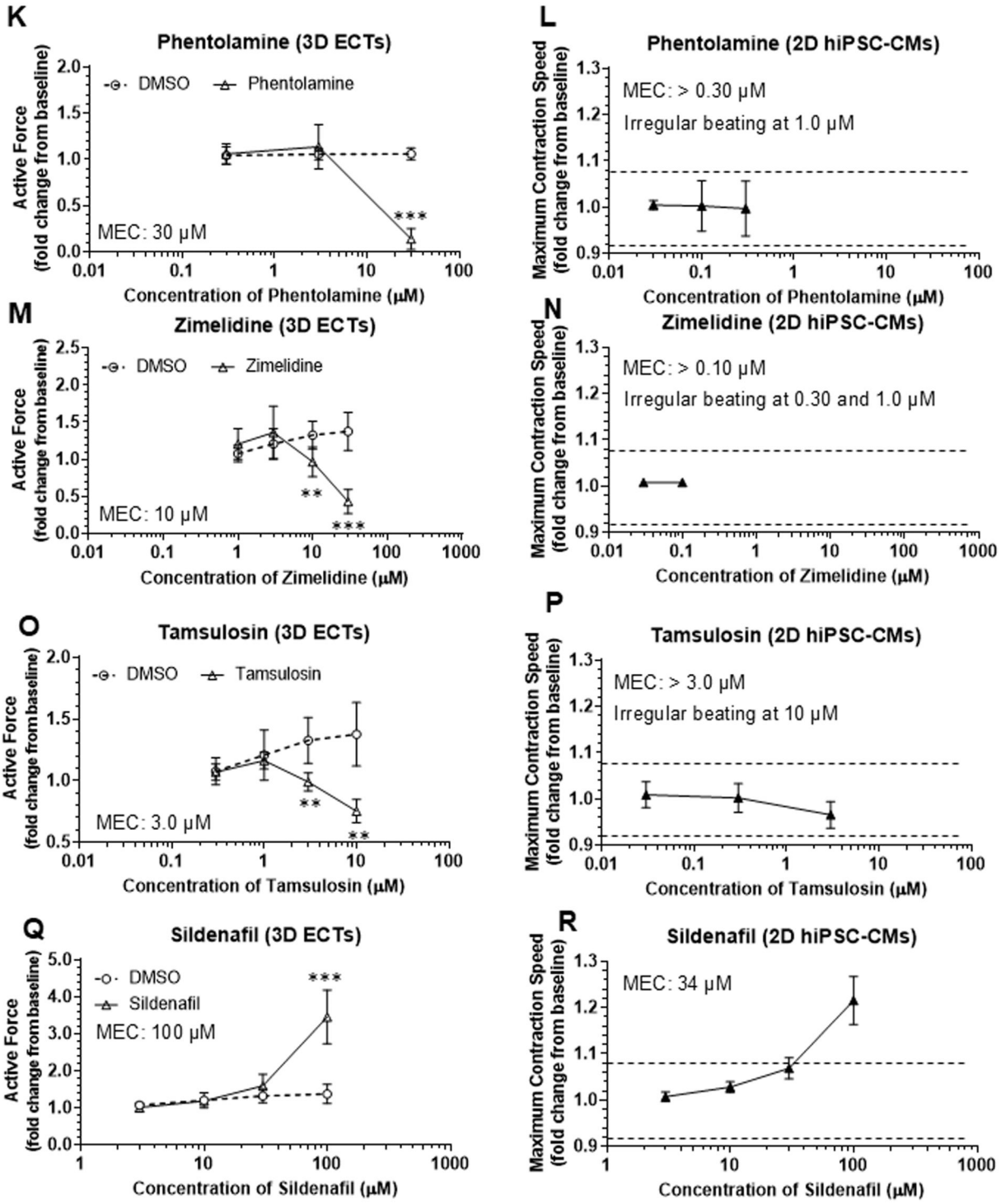

Fig. 4. Continued

profiling select candidate compounds and/or mechanistic investigations of hemodynamic changes observed in the in vivo or clinical studies.

In conclusion, this study provides a comparison between 3D ECTs and 2D hiPSC-CMs for contractility assessment. Several positive and negative inotropes that were not detected in 2D hiPSC-CMs were successfully identified in 3D ECTs. Furthermore, gene expression analysis suggested that the enhanced maturity of 3D ECTs may contribute to their improved detection capability.

Acknowledgments

The authors would like to thank Dr Hisakazu Komori and Dr Matthew Wagoner for helpful discussions and insights.

Supplementary material

Supplementary material is available at *Toxicological Sciences* online.

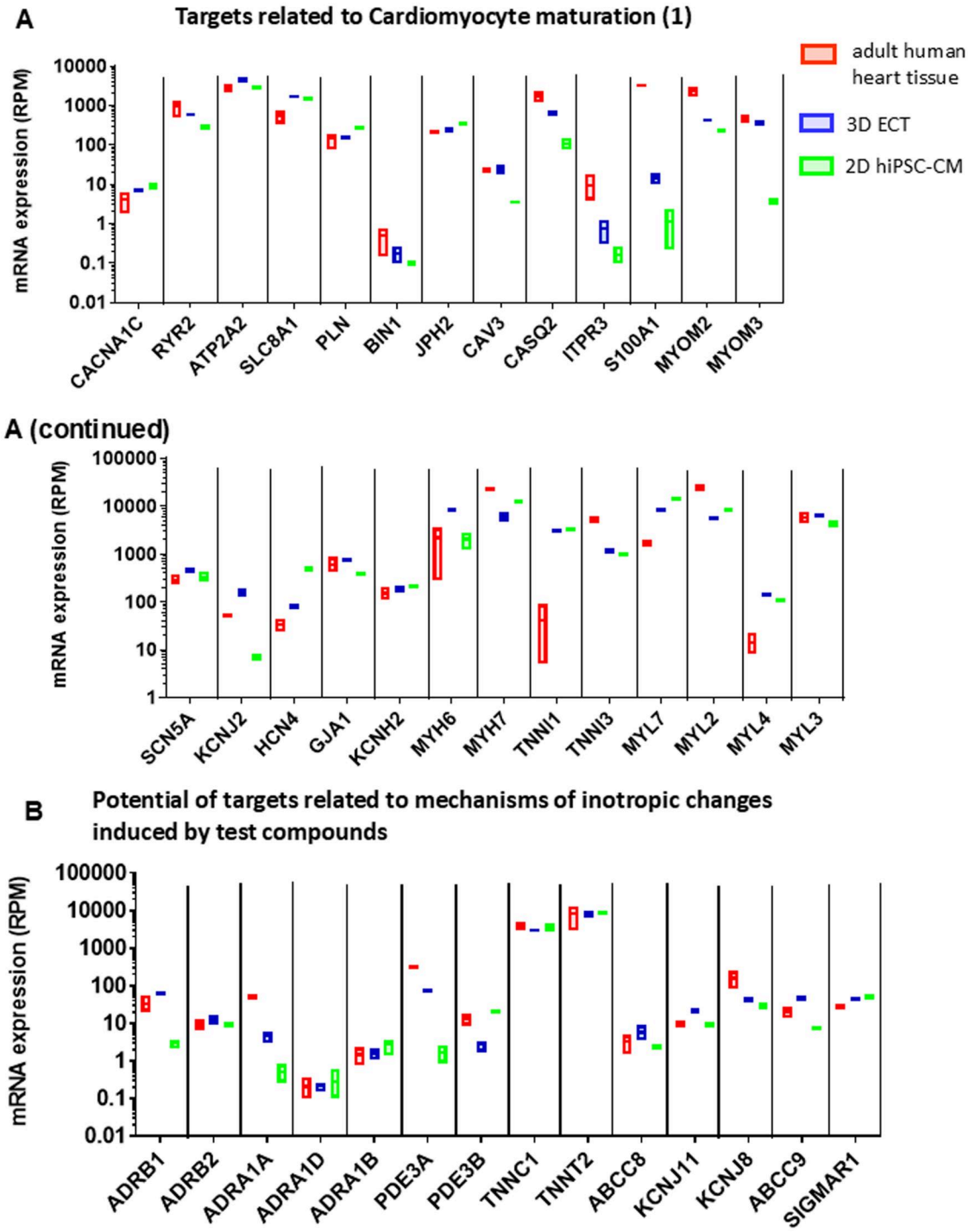

Fig. 5. Comparison of gene expression levels among the adult human heart tissue, the 3D ECTs, and the 2D hiPSC-CMs determined based on RNA sequencing. A) Gene expression of cardiomyocyte maturation-related targets. B) Gene expression levels of potential targets related to the mechanisms underlying test compound-induced inotropy.

Funding

This study did not receive any specific grants from funding agencies in the public, commercial, or non-profit sectors.

Disclosures. NF and IP are employees and shareholders of Valo Health.

Conflicts of interest. None declared.

References

Ahmad SR, Singer SJ, Leissa BG. 2001. Congestive heart failure associated with itraconazole. Lancet. 357:1766–1767.

Ahmad T, Miller PE, McCullough M, Desai NR, Riello R, Psotka M, Bohm M, Allen LA, Teerlink JR, Rosano GMC, *et al.* 2019. Why has positive inotropy failed in chronic heart failure? Lessons from prior inotrope trials. Eur J Heart Fail. 21:1064–1078.

Ando H, Yoshinaga T, Yamamoto W, Asakura K, Uda T, Taniguchi T, Ojima A, Shinkyo R, Kikuchi K, Osada T, *et al.* 2017. A new paradigm for drug-induced torsadogenic risk assessment using human ips cell-derived cardiomyocytes. J Pharmacol Toxicol Methods. 84:111–127.

Beca S, Ahmad F, Shen W, Liu J, Makary S, Polidovitch N, Sun J, Hockman S, Chung YW, Movsesian M, *et al.* 2013. Phosphodiesterase type 3a regulates basal myocardial contractility through interacting with sarcoplasmic reticulum calcium atpase type 2a signaling complexes in mouse heart. Circ Res. 112:289–297.

Bryant SM, Kong CHT, Watson JJ, Gadeberg HC, Roth DM, Patel HH, Cannell MB, James AF, Orchard CH. 2018. Caveolin-3 ko disrupts t-tubule structure and decreases t-tubular i(ca) density in mouse ventricular myocytes. Am J Physiol Heart Circ Physiol. 315: H1101–H1111.

Burridge PW, Li YF, Matsa E, Wu H, Ong SG, Sharma A, Holmstrom A, Chang AC, Coronado MJ, Ebert AD, *et al.* 2016. Human induced pluripotent stem cell-derived cardiomyocytes recapitulate the predilection of breast cancer patients to doxorubicin-induced cardiotoxicity. Nat Med. 22:547–556.

Ernst P, Bidwell PA, Dora M, Thomas DD, Kamdar F. 2022. Cardiac calcium regulation in human induced pluripotent stem cell cardiomyocytes: implications for disease modeling and maturation. Front Cell Dev Biol. 10:986107.

Feric NT, Pallotta I, Singh R, Bogdanowicz DR, Gustilo MM, Chaudhary KW, Willette RN, Chendrimada TP, Xu X, Graziano MP, *et al.* 2019. Engineered cardiac tissues generated in the biowire ii: a platform for human-based drug discovery. Toxicol Sci. 172:89–97.

Fuentes AV, Pineda MD, Venkata KCN. 2018. Comprehension of top 200 prescribed drugs in the us as a resource for pharmacy teaching, training and practice. Pharmacy (Basel). 6:43.

Hatip-Al-Khatib I, Bolukbaşi-Hatip F. 2002. Modulation of the negative inotropic effect of haloperidol by drugs with positive inotropic effects in isolated rabbit heart. Pharmacology. 66:19–25.

Hayakawa T, Kunihiro T, Dowaki S, Uno H, Matsui E, Uchida M, Kobayashi S, Yasuda A, Shimizu T, Okano T. 2012. Noninvasive evaluation of contractile behavior of cardiomyocyte monolayers based on motion vector analysis. Tissue Eng Part C Methods. 18:21–32.

Hinata Y, Kagawa Y, Kubo H, Kato E, Baba A, Sasaki D, Matsuura K, Sawada K, Shimizu T. 2022. Importance of beating rate control for the analysis of drug effects on contractility in human induced pluripotent stem cell-derived cardiomyocytes. J Pharmacol Toxicol Methods. 118:107228.

Hori Y, Taira H, Nakajima Y, Ishikawa Y, Yumoto Y, Maekawa Y, Oshiro A. 2019. Inotropic effects of a single intravenous recommended dose of pimobendan in healthy dogs. J Vet Med Sci. 81:22–25.

Karbassi E, Fenix A, Marchiano S, Muraoka N, Nakamura K, Yang X, Murry CE. 2020. Cardiomyocyte maturation: advances in knowledge and implications for regenerative medicine. Nat Rev Cardiol. 17:341–359.

Laverty H, Benson C, Cartwright E, Cross M, Garland C, Hammond T, Holloway C, McMahon N, Milligan J, Park B, *et al.* 2011. How can we improve our understanding of cardiovascular safety liabilities to develop safer medicines? Br J Pharmacol. 163:675–693.

Law CW, Chen Y, Shi W, Smyth GK. 2014. Voom: precision weights unlock linear model analysis tools for RNA-seq read counts. Genome Biol. 15:R29.

Lubna NJ, Nakamura Y, Cao X, Wada T, Izumi-Nakaseko H, Ando K, Sugiyama A. 2016. Cardiac safety profile of sildenafil: chronotropic, inotropic and coronary vasodilator effects in the canine isolated, blood-perfused heart preparations. J Toxicol Sci. 41:739–744.

Ma J, Guo L, Fiene SJ, Anson BD, Thomson JA, Kamp TJ, Kolaja KL, Swanson BJ, January CT. 2011. High purity human-induced pluripotent stem cell-derived cardiomyocytes: electrophysiological properties of action potentials and ionic currents. Am J Physiol Heart Circ Physiol. 301:H2006–2017.

Machiraju P, Greenway SC. 2019. Current methods for the maturation of induced pluripotent stem cell-derived cardiomyocytes. World J Stem Cells. 11:33–43.

Movsesian M, Ahmad F, Hirsch E. 2018. Functions of pde3 isoforms in cardiac muscle. J Cardiovasc Dev Dis. 5:10.

Nachimuthu S, Assar MD, Schussler JM. 2012. Drug-induced qt interval prolongation: Mechanisms and clinical management. Ther Adv Drug Saf. 3:241–253.

Novakova M, Ela C, Barg J, Vogel Z, Hasin Y, Eilam Y. 1995. Inotropic action of sigma receptor ligands in isolated cardiac myocytes from adult rats. Eur J Pharmacol. 286:19–30.

Okai Y, Matsune K, Yamanaka K, Matsui T, Pfeiffer Kaushik E, Harada K, Kohara H, Miyawaki A, Ozaki H, Wagoner M, *et al.* 2020. Video-based assessment of drug-induced effects on contractile motion properties using human induced pluripotent stem cell-derived cardiomyocytes. J Pharmacol Toxicol Methods. 105:106893.

Parton RG, Way M, Zorzi N, Stang E. 1997. Caveolin-3 associates with developing t-tubules during muscle differentiation. J Cell Biol. 136:137–154.

Qu Y, Fang M, Gao B, Amouzadeh HR, Li N, Narayanan P, Acton P, Lawrence J, Vargas HM. 2013. Itraconazole decreases left ventricular contractility in isolated rabbit heart: mechanism of action. Toxicol Appl Pharmacol. 268:113–122.

Qu Y, Feric N, Pallotta I, Singh R, Sobbi R, Vargas HM. 2020. Inotropic assessment in engineered 3d cardiac tissues using human induced pluripotent stem cell-derived cardiomyocytes in the biowiretm ii platform. J Pharmacol Toxicol Methods. 105:106886.

Rajapreyar IN, Ennezat PV, Le Jemtel TH. 2014. Toward safe inotropic therapy. J Cardiovasc Pharmacol. 64:385–392.

Ribeiro AJS, Guth BD, Engwall M, Eldridge S, Foley CM, Guo L, Gintant G, Koerner J, Parish ST, Pierson JB, *et al.* 2019. Considerations for an in vitro, cell-based testing platform for detection of drug-induced inotropic effects in early drug development. Part 2: designing and fabricating microsystems for assaying cardiac contractility with physiological relevance using human iPSC-cardiomyocytes. Front Pharmacol. 10:934.

Ronaldson-Bouchard K, Ma SP, Yeager K, Chen T, Song L, Sirabella D, Morikawa K, Teles D, Yazawa M, Vunjak-Novakovic G. 2018. Advanced maturation of human cardiac tissue grown from pluripotent stem cells. Nature. 556:239–243.

Saleem U, van Meer BJ, Katili PA, Mohd Yusof NAN, Mannhardt I, Garcia AK, Tertoolen L, de Korte T, Vlaming MLH, McGlynn K, *et al.* 2020. Blinded, multicenter evaluation of drug-induced changes in contractility using human-induced pluripotent stem cell-derived cardiomyocytes. Toxicol Sci. 176:103–123.

Satsuka A, Ribeiro AJS, Kawagishi H, Yanagida S, Hirata N, Yoshinaga T, Kurokawa J, Sugiyama A, Strauss DG, Kanda Y. 2024. Contractility assessment using aligned human ipsc-derived cardiomyocytes. J Pharmacol Toxicol Methods. 128:107530.

Scott CW, Zhang X, Abi-Gerges N, Lamore SD, Abassi YA, Peters MF. 2014. An impedance-based cellular assay using human iPSC-derived cardiomyocytes to quantify modulators of cardiac contractility. Toxicol Sci. 142:331–338.

Siramshetty VB, Nickel J, Omieczynski C, Gohlke BO, Drwal MN, Preissner R. 2016. Withdrawn—a resource for withdrawn and discontinued drugs. Nucleic Acids Res. 44:D1080–1086.

Sube R, Ertel EA. 2017. Cardiomyocytes derived from human induced pluripotent stem cells: an in-vitro model to predict cardiac effects of drugs. JBiSE. 10:527–549.

Tadano K, Miyagawa S, Takeda M, Tsukamoto Y, Kazusa K, Takamatsu K, Akashi M, Sawa Y. 2021. Cardiotoxicity assessment using 3d vascularized cardiac tissue consisting of human ipsc-derived cardiomyocytes and fibroblasts. Mol Ther Methods Clin Dev. 22:338–349.

Takada T, Sasaki D, Matsuura K, Miura K, Sakamoto S, Goto H, Ohya T, Iida T, Homma J, Shimizu T, *et al.* 2022. Aligned human induced pluripotent stem cell-derived cardiac tissue improves contractile properties through promoting unidirectional and synchronous cardiomyocyte contraction. Biomaterials. 281:121351.

van Meer BJ, Krotenberg A, Sala L, Davis RP, Eschenhagen T, Denning C, Tertoolen LGJ, Mummery CL. 2019. Simultaneous measurement of excitation-contraction coupling parameters identifies mechanisms underlying contractile responses of hiPSC-derived cardiomyocytes. Nat Commun. 10:4325.

Wallis R, Gharanei M, Maddock H. 2015. Predictivity of in vitro non-clinical cardiac contractility assays for inotropic effects in humans—a literature search. J Pharmacol Toxicol Methods. 75:62–69.

Wang DW, Mistry AM, Kahlig KM, Kearney JA, Xiang J, George AL Jr. 2010. Propranolol blocks cardiac and neuronal voltage-gated sodium channels. Front Pharmacol. 1:144.

Waring MJ, Arrowsmith J, Leach AR, Leeson PD, Mandrell S, Owen RM, Pairaudeau G, Pennie WD, Pickett SD, Wang J, *et al.* 2015. An analysis of the attrition of drug candidates from four major pharmaceutical companies. Nat Rev Drug Discov. 14:475–486.

Zhao Y, Rafatian N, Feric NT, Cox BJ, Aschar-Sobbi R, Wang EY, Aggarwal P, Zhang B, Conant G, Ronaldson-Bouchard K, *et al.* 2019. A platform for generation of chamber-specific cardiac tissues and disease modeling. Cell. 176:913–927 e918.

Toxicological Sciences, 2025, 205, 401–416
https://doi.org/10.1093/toxsci/kfaf033
Research article